

**Technical Report No. 32-189**

**Thermal and Criticality Analysis of the  
Plasma Core Reactor**

**D. F. Spencer**



**JET PROPULSION LABORATORY  
CALIFORNIA INSTITUTE OF TECHNOLOGY  
PASADENA, CALIFORNIA**

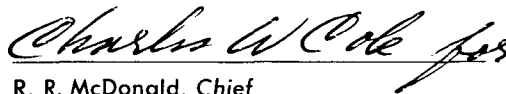
January 1, 1962

NATIONAL AERONAUTICS AND SPACE ADMINISTRATION  
CONTRACT No. NASW-6

Technical Report No. 32-189

**Thermal and Criticality Analysis of the  
Plasma Core Reactor**

D. F. Spencer



R. R. McDonald, Chief  
Engineering Research

JET PROPULSION LABORATORY  
CALIFORNIA INSTITUTE OF TECHNOLOGY  
PASADENA, CALIFORNIA

January 1, 1962

Copyright © 1961  
Jet Propulsion Laboratory  
California Institute of Technology

CONTENTS

I. Thermal Analysis .....	1
II. Criticality Analysis .....	13
III. Superposition of Results from Parts I and II .....	28
References .....	31
Nomenclature to Part I and Appendix A .....	11
Nomenclature to Part II and Appendixes B, C, D, and E .....	26
Appendixes	
A. Calculation of Temperature Distribution in the Propellant .....	32
B. Application of Continuity Conditions on Thermal and Fast Currents .....	38
C. Evaluation of Integral Form for $P_m$ .....	42
D. Determination of the Final Equations for Fast and Thermal Fluxes in the Reflector .....	44
E. Summary of Nuclear Parameters Used in the Analysis .....	46

FIGURES

1. Emissivity per unit length of hydrogen vs temperature .....	2
2. Schematic indicating hydrogen zones used in thermal analysis.....	5
3. Graphical determination of maximum hydrogen temperature and hydrogen thickness.....	9
4. Engine specific impulse vs required hydrogen thickness .....	10
5. Steady-state temperature profile in hydrogen .....	10
6. The three regions of a gaseous core reactor.....	13
7. Geometric path length of neutron penetrating the core .....	20
8. Critical fuel concentration vs $r_c/r_r$ for $T = 100$ cm .....	22
9. Critical fuel concentration vs $r_c/r_r$ for $T = 200$ cm .....	22

FIGURES (Cont'd)

10. Critical mass vs $r_c/r_r$ for $T = 100$ cm.....	23
11. Critical mass vs $r_c/r_r$ for $T = 200$ cm.....	23
12. Flux distribution in reflector ( $r_c = 300$ cm, $r_r = 500$ cm, $T = 100$ cm).....	24
13. Flux distribution in reflector ( $r_c = 300$ cm, $r_r = 600$ cm, $T = 100$ cm).....	24
14. Flux distribution in reflector ( $r_c = 300$ cm, $r_r = 600$ cm, $T = 200$ cm).....	25
15. Maximum achievable engine specific impulse based on thermal and criticality constraints ( $T_c \geq 20,000^\circ\text{K}$ ) .....	28
16. Achievable engine thrust based on thermal and criticality constraints ( $T_c \geq 20,000^\circ\text{K}$ ).....	29

## ABSTRACT

Radiative heat transfer to the propellant and reactor criticality for a fissionable gaseous rocket engine are analyzed to determine their interdependence. The necessity for propellant thicknesses of approximately 1-3 m due to poor thermal absorption properties of hydrogen significantly affects reactor critical radius and mass. The two primary adverse effects are: (1) increased absorption in the reflector-moderator for a given reflector thickness and (2) poor utilization of thermal neutrons by the core due to the lower geometrical view factor of the core for the reflector walls. In fact, there is a minimum core radius at a particular propellant thickness which allows the system to "go" critical.

Engine performance is limited primarily to two regions of operation: the first, a specific impulse of approximately 1550 sec at a thrust level of  $2 \times 10^6$  lb and second, a specific impulse of approximately 2200 sec at a thrust level of  $5.3 \times 10^6$  lb.

## I. THERMAL ANALYSIS

The utilization of a high-temperature gaseous fission reactor as a source of energy for nuclear rocket propulsion is based on the direct interchange of energy between the fissionable material and the propellant. In the case of the plasma core reactor (Ref. 1) and the coaxial flow reactor (Ref. 2), the principal mechanism of interchange is due to thermal radiation from fuel to propellant. (Although not described in the Report, it is

relatively easy to show that convective exchange of energy from plasma to propellant is less than 1% of the radiative mechanism and fission-fragment heating less than 5%.) In order to effect this interchange, and thereby heat the propellant to a high temperature, the opacity of the propellant must be sufficiently high to absorb the thermal radiation emitted by the fissionable material.

The propellant temperature at injection into the cavity region is limited by the maximum operating temperature of the reflector-moderator (henceforth to be referred to simply as the reflector). The discussion will be limited to a graphite reflector, with a peak operating temperature of 2500°K. The maximum obtainable propellant temperature is restricted by the fact that part of the fission energy is deposited directly in the graphite as neutron and gamma heating. This energy, and, in addition, any thermal energy reaching the reflector, must be absorbed by the propellant prior to injection into the cavity (Ref. 3).

The principal difficulty in the transfer of energy from core (plasma) to propellant is the high transparency of the propellant, hydrogen, for thermal radiation in the temperature range 2500–8000°K. Figure 1 shows the emissivity per unit length of hydrogen versus temperature, as calculated from the data of Olfe (Ref. 4) for a pressure of 30 atm.

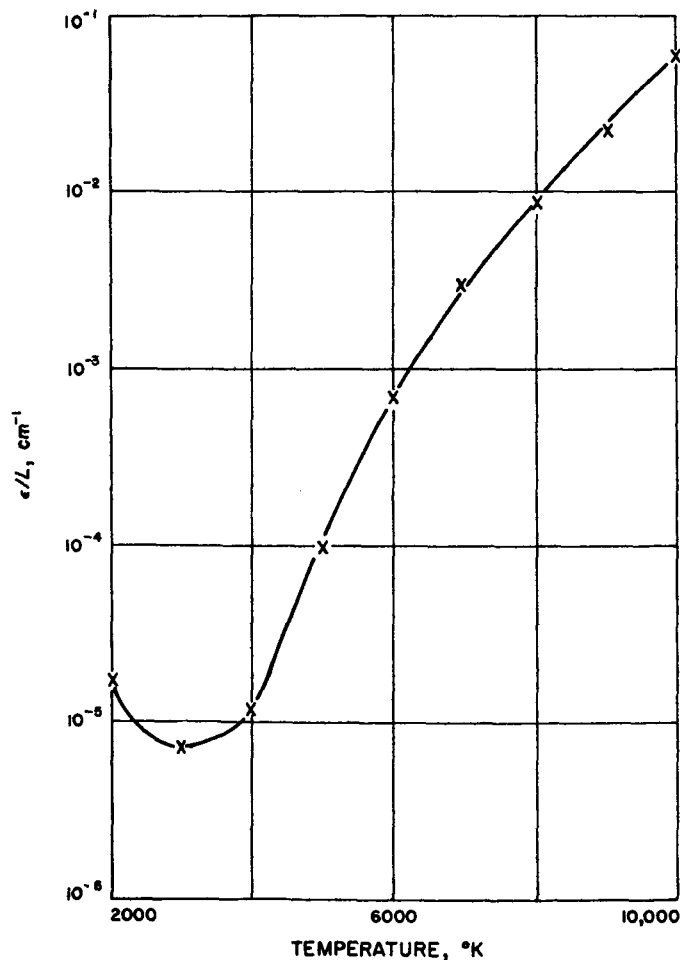


Fig. 1. Emissivity per unit length of hydrogen vs temperature

In order to heat the hydrogen by thermal radiation, it must be seeded by some solid material over at least a portion of this temperature range to increase its apparent absorptivity. In the following analysis, tantalum carbide in particulate form was assumed to be added to the hydrogen. The weight-percent TaC in the hydrogen is restricted to 2%, based on the maximum hydrogen temperature in the cavity, so that it does not appreciably affect the specific impulse of the engine.

The primary objectives of the thermal analysis are to obtain:

1. The thickness of propellant necessary to heat the hydrogen from the wall temperature to its maximum chamber temperature.
2. The maximum obtainable propellant temperature (specific impulse) as a function of flow rate.
3. The steady-state temperature profile in the propellant for various plasma temperatures and radii.

The above objectives are attained by requiring the enthalpy rise in the cavity to be consistent with the rise in the reflector.

In order to perform the analysis, certain simplifying assumptions have been made:

1. The plasma radiates at an average temperature  $T_p$  as a black body.
2. The wall radiates as a black body at  $T_w = 2500^\circ\text{K}$ .
3. The plasma, propellant, and wall are concentric spheres.
4. Hydrogen is a gray gas and opaque to all wavelengths when seeded.
5. The seeding agent is effective to its sublimation temperature but does not affect the absorptivity above this temperature.
6. The seeding agent considered, TaC, sublimates at  $5800^\circ\text{K}$  and has thermal absorption properties similar to graphite to this temperature.
7. The hydrogen enters the chamber radially, and the total path length to heat it to the maximum chamber temperature is the inner reflector radius minus the core radius,  $R_r - R_c$ .



8. Direct heating of the propellant by fission fragments and convective heat transfer can be neglected (< 6%).

9. Engine performance is based on a 20:1 expansion ratio of the nozzle.

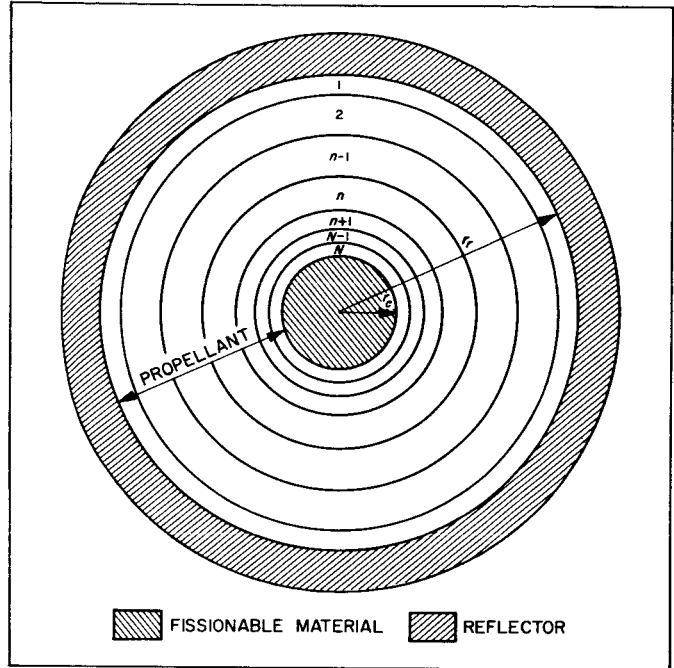
Using assumption 8, the net heat input to the  $n$ th zone of hydrogen,  $n$  running from 1 at the reflector to  $N$  at the plasma surface (Fig. 2), is given by

$$\begin{aligned}
 (Q_{\text{net},p})_n &= F_{c,n} \sigma A_c T_c^4 \alpha_n^{T_c} [(1 - \alpha_N^{T_c})(1 - \alpha_{N-1}^{T_c})(1 - \alpha_{N-2}^{T_c}) \cdots (1 - \alpha_{n+1}^{T_c})] \\
 &+ F_{N,n} \sigma \bar{A}_N \bar{T}_N^4 \epsilon_N^{T_N} \alpha_n^{\bar{T}_N} [(1 - \alpha_{N-1}^{\bar{T}_N})(1 - \alpha_{N-2}^{\bar{T}_N}) \cdots (1 - \alpha_{n+1}^{\bar{T}_N})] \\
 &+ \cdots + F_{n+1,n} \sigma \bar{A}_{n+1} \bar{T}_{n+1}^4 \epsilon_{n+1}^{\bar{T}_{n+1}} \alpha_n^{\bar{T}_{n+1}} - [\sigma \bar{A}_n \bar{T}_n^4 \epsilon_n^{\bar{T}_n}] \\
 &\times [F_{n,c} (1 - \alpha_N^{\bar{T}_n})(1 - \alpha_{N-1}^{\bar{T}_n}) \cdots (1 - \alpha_{n+1}^{\bar{T}_n}) + F_{n,N} (1 - \alpha_{N-1}^{\bar{T}_n}) \\
 &\quad \times (1 - \alpha_{N-2}^{\bar{T}_n}) \cdots (1 - \alpha_{n+1}^{\bar{T}_n}) + \cdots + F_{n,n+1}] + F_{r,n} \sigma A_r T_r^4 \alpha_n^{T_r} \quad (1) \\
 &\times [(1 - \alpha_{n-1}^{T_r})(1 - \alpha_{n-2}^{T_r}) \cdots (1 - \alpha_1^{T_r})] - F_{n,r} \sigma \bar{A}_n \bar{T}_n^4 \epsilon_n^{\bar{T}_n} \\
 &\times [(1 - \alpha_{n-1}^{\bar{T}_n})(1 - \alpha_{n-2}^{\bar{T}_n}) \cdots (1 - \alpha_1^{\bar{T}_n})] + \alpha_n^{\bar{T}_{n-1}} \epsilon_{n-1}^{\bar{T}_{n-1}} \bar{A}_{n-1} \bar{T}_{n-1}^4 F_{n-1,n} \\
 &+ \alpha_n^{\bar{T}_{n-2}} \epsilon_{n-2}^{\bar{T}_{n-2}} \sigma \bar{A}_{n-2} \bar{T}_{n-2}^4 F_{n-2,n} (1 - \alpha_{n-1}^{\bar{T}_{n-2}}) + \cdots + \alpha_n^{\bar{T}_1} \epsilon_1^{\bar{T}_1} \sigma \bar{A}_1 \bar{T}_1^4 F_{1,n} \\
 &\times (1 - \alpha_{n-1}^{\bar{T}_1}) \cdots (1 - \alpha_2^{\bar{T}_1}) - \sigma \bar{A}_n \bar{T}_n^4 \epsilon_n^{\bar{T}_n} \{F_{n,n-1} + F_{n,n-2} (1 - \alpha_{n-1}^{\bar{T}_n}) \\
 &\quad + \cdots + F_{n,1} [(1 - \alpha_{n-1}^{\bar{T}_n})(1 - \alpha_{n-2}^{\bar{T}_n}) \cdots (1 - \alpha_2^{\bar{T}_n})]\}
 \end{aligned}$$

It is required that the net heat input to the  $n$ th zone be sufficient to heat it from  $T_{n-1}$  to  $T_n$ . Thus,

$$(Q_{\text{net},p})_n = \dot{w}_p \Delta H_n \quad (2)$$

Fig. 2. Schematic indicating hydrogen zones used in thermal analysis



Further, the enthalpy rise in the propellant prior to injection into the cavity is determined by the total heat reaching the reflector as nuclear and thermal heating:

$$\dot{w}_p (H_{T_r} - H_l) = \dot{w}_p \Delta H_r = \left[ \frac{\delta_N}{1 - \delta_N} + \delta_{th} \right] Q \quad (3)$$

and the total enthalpy rise in the cavity must equal the total thermal energy emitted by the plasma, minus the contribution which reaches the wall. Then,

$$\dot{w}_p (H_{T_N} - H_{T_r}) = \dot{w}_p \Delta H_{p,c} = \sum_{n=1}^N \dot{w}_p \Delta H_n = (1 - \delta_{th}) Q \quad (4)$$

Combination of Eqs. (3) and (4) yields

$$\frac{\Delta H_{p,c}}{\Delta H_r} = \frac{1 - \delta_{th}}{\frac{\delta_N}{1 - \delta_N} + \delta_{th}} \quad (5)$$

Since the allowable enthalpy rise in the walls and  $\delta_N$  are fixed, there is a maximum enthalpy rise of the propellant in the cavity for  $\delta_{th} = 0$  which limits the peak propellant temperature  $(T_p)_{\max}$ . For any  $\delta_{th} > 0$ , the maximum obtainable propellant temperature is less than this value.

In most cases of interest, the energy emitted directly by the plasma and attenuated within the propellant is the dominant heat source for each layer; i.e.,  $T_c^4 \gg T_n^4$ . This allows one to neglect radiative transfer from one zone to another within the propellant and from the reflector to the propellant, thus simplifying tremendously the calculational procedure. Even when the plasma temperature is only twice the maximum propellant temperature, emission from the  $N$ th zone of hydrogen is unimportant.

Using assumptions 1, 2, 3, 4, and 5 and the result from the preceding paragraph,

$$(Q_{\text{net},p})_n = \epsilon_n^{\bar{T}_n} \sigma A_c [(1 - \epsilon_N^{T_N})(1 - \epsilon_{N-1}^{T_{N-1}}) \dots (1 - \epsilon_{n+1}^{T_{n+1}})] (T_c^4 - \bar{T}_n^4) - \epsilon_n^{\bar{T}_n} \sigma \bar{A}_n T_n^4 \quad (6)$$

Equation (6) provides a conservative estimate of the heating for each zone, thus giving the maximum thickness required. In order to determine the thickness of each zone, substitute Eq. (2) into (6) and express  $\epsilon_n^{\bar{T}_n}$  as  $(\epsilon/L)^{\bar{T}_n} (\Delta r)_n$ . Then, Eq. (6) becomes

$$\begin{aligned} \dot{w}_p \Delta H_n &= \left(\frac{\epsilon}{L}\right)^{\bar{T}_n} (\Delta r)_n \sigma A_c (T_c^4 - \bar{T}_n^4) [(1 - \epsilon_N^{T_N})(1 - \epsilon_{N-1}^{T_{N-1}}) \dots (1 - \epsilon_{n+1}^{T_{n+1}})] \\ &\quad - \left(\frac{\epsilon}{L}\right)^{\bar{T}_n} \Delta r_n \sigma A_m \bar{T}_n^4 \end{aligned} \quad (7)$$

Solution to this equation can be obtained by a procedure which is demonstrated in Appendix A. Since the energy input to layer  $n$  is dependent on the transmission properties of other layers nearer the plasma, the calculation begins for  $n = N$  and continues toward the wall. In this way, the attenuation from previous layers is automatically taken into account.

This procedure may be utilized for propellant temperatures above the sublimation temperature of the seeding agent and, in fact, may be utilized to obtain the total absorptivity required in the zone; i.e., the zone in which the propellant is heated from the wall temperature to the sublimation temperature of the seeding agent.

In this case, we have

$$\dot{w}_p (\Delta H_1) = \alpha_1 \sigma A_c T_c^4 (1 - \epsilon_N^{T_N}) (1 - \epsilon_{N-1}^{T_{N-1}}) \dots (1 - \epsilon_2^{T_2}) = \alpha_1 Q_1 \quad (8)$$

Then,

$$\alpha_1 = \frac{\dot{w}_p \Delta H_1}{Q_1} \quad (9)$$

The procedure to obtain  $\Delta r_1$  is that given by Barre (Ref. 5), coupled with assumption 6.

Now,

$$(1 - \alpha_1) = \frac{Q_r}{Q_1} \quad (10)$$

and, from Ref. 5,

$$\ln \frac{Q_1}{Q_r} = \mu \Delta r_1 \quad (11)$$

From the assumption that the plasma radiates as a black body, Wien's Law gives

$$\lambda_{T_c} = \frac{0.293}{T_c} \quad (12)$$

The plot of  $\log \mu / (\pi r_s^2 N_s)$  versus  $\log r_s / \lambda_{T_c}$  (Fig. 4 of Ref. 5) gives a relation of the form

$$\mu = K \pi r_s^2 N_s \quad (13)$$

where  $K$  may be evaluated (from this figure) for a given  $r_s / \lambda_{T_c}$ .

Combining Eqs. (11) and (12) and solving for  $N_s$ ,

$$N_s = \frac{\ln \frac{Q_r}{Q_1}}{K \pi r_s^2 \Delta r_1} \quad (14)$$

The mass of a TaC particle is

$$m_s = \left( \frac{4}{3} \pi r_s^3 \right) (\rho_s) \quad (15)$$

It is obvious that  $\Delta r_1$  can be made as small as we wish by simply increasing  $N_s$ . But it has been assumed that the weight fraction of TaC should be only 2%. Then,

$$\frac{N_s (m_s)}{\rho_p} = 0.02 \quad (16)$$

Substituting Eqs. (15) and (16) into (14) and solving for  $\Delta r_1$ ,

$$\Delta r_1 = \frac{67}{K} r_s \frac{\rho_s}{\rho_p} \ln \frac{Q_1}{Q_r} \quad (17)$$

This provides the final increment in  $\Delta r$ . The sum of the  $\Delta r$  gives the total hydrogen thickness, or, from assumption 7, the difference between the reflector and core radii:

$$r_r - r_c = \sum_{n=1}^N \Delta r_n \quad (18)$$

Since  $\alpha_1 Q_1$  is known from Eq. (8), the actual fraction of thermal energy reaching the wall,  $(\delta_{th})_a$ , can be calculated.

$$(\delta_{th})_a = \frac{Q_r}{Q_c} = \frac{(1 - \alpha_1) Q_1}{Q_c} \quad (19)$$

To obtain a solution for a particular flow rate and maximum hydrogen temperature, the value of  $(\delta_{th})_a$  must be consistent with  $\delta_{th}$  calculated from Eq. (5) for a given ratio of  $\Delta H_{p,c}/\Delta H_r$ . The method of obtaining the correct hydrogen thickness and maximum propellant temperature for a given flow rate is demonstrated in Fig. 3 (for details see Appendix A) by a graphical procedure for  $T_c = 30,000^\circ\text{K}$ ,  $\dot{w}_p = 1.36 \times 10^6$  g/sec, and  $r_c = 100$  cm. The required hydrogen thickness ( $r_r - r_c$ ) is 292 cm, and the hydrogen has a peak temperature of  $10,800^\circ\text{K}$ , which corresponds to an engine specific impulse of 1900 sec for a 20:1 expansion ratio of the nozzle (Ref. 6).

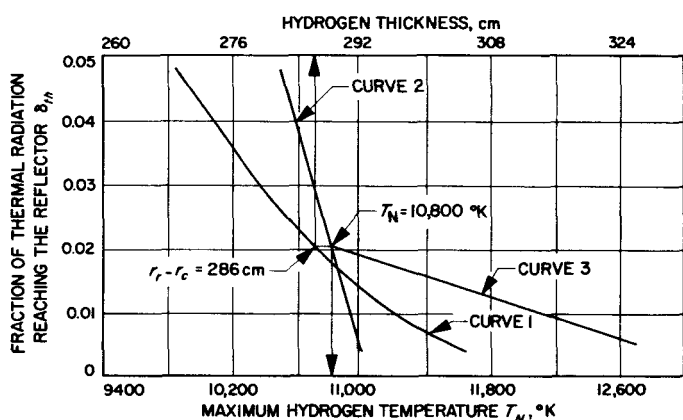
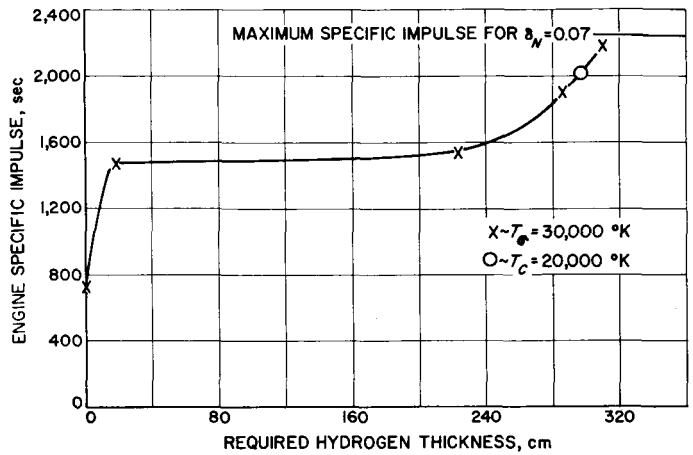


Fig. 3. Graphical determination of maximum hydrogen temperature and hydrogen thickness

A similar procedure was used to obtain the curve in Fig. 4, which presents the engine specific impulse as a function of required hydrogen thickness. This curve is valid for any plasma radius, as shown in Appendix A, and to calculational accuracy is independent of core temperature above  $20,000^\circ\text{K}$ . Of course, the flow rate necessary to cool the engine depends on the plasma temperature and radius.

The significant feature of Fig. 4 is the appreciable thickness of hydrogen necessary to heat the propellant from  $5800^\circ\text{K}$  to  $8000^\circ\text{K}$ . This exemplifies the very poor thermal radiative-absorption characteristics of hydrogen. In fact, a similar analysis using graphite as the seeding agent requires thicknesses of approximately 300 m to heat the hydrogen from the graphite sublimation temperature ( $4000^\circ\text{K}$ ) to  $5000^\circ\text{K}$ . This may prohibit seeding with graphite in the high-temperature application of this system.

Fig. 4. Engine specific impulse vs required hydrogen thickness



From the results shown in Fig. 4, it appears that engine performance will be limited to two regions of operation; namely, (1) specific impulse below 1500 sec, with approximately 20 cm of hydrogen or (2) a specific impulse in the range of 2000–2500 sec, with hydrogen thicknesses of approximately 300 cm. The reflection of this result on critical mass and radius will be considered in the second part of this Report. The effect on over-all engine and system performance will be the subject of a later Report by the author.

Figure 5 shows the steady-state temperature distribution in the hydrogen for a flow rate of 3000 lb/sec and a specific impulse of 1900 sec. As would be expected, it has a form similar to that in Fig. 4 and reiterates the difficulty of heating hydrogen from 5800 to 8000°K.

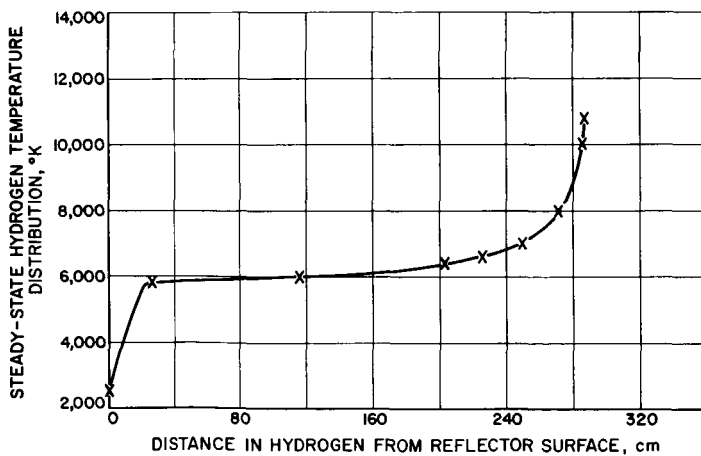


Fig. 5. Steady-state temperature profile in hydrogen

**NOMENCLATURE**  
(Part I and Appendix A)

$A$	thermal-energy emittance area, $\text{cm}^2$
$\bar{A}$	average emittance area, $\text{cm}^2$
$F$	view factor $F_{12}$ = fraction of radiation emitted by area one, intercepted directly by area two
$H$	enthalpy, $\text{cal/g}$
$K$	arbitrary constant, dimensionless
$L$	diffusion length, $\text{cm}$
$m$	particle mass, $\text{g}$
$N$	particle concentration, $\text{particles/cm}^3$
$Q$	heat input, $\text{cal/sec}$
$r$	radius, $\text{cm}$
$T$	temperature, $^\circ\text{K}$
$\bar{T}$	average temperature, $^\circ\text{K}$
$\dot{w}_p$	propellant flow rate, $\text{g/sec}$
$\alpha$	thermal-radiation absorptivity
$\Delta H$	enthalpy change, $\text{cal/lb}$
$\Delta r$	radial-distance increment, $\text{cm}$
$\delta_N$	nuclear-radiation fraction of fission energy (gamma and neutron energy)
$\delta_{th}$	fraction of radiated energy reaching reflector
$\epsilon$	thermal-radiation emissivity
$\lambda$	wavelength at peak of black-body radiation curve, $\text{cm}$
$\mu$	absorption coefficient per unit length of seed material, $\text{cm}^{-1}$
$\rho$	density, $\text{g/cm}^3$
$\sigma$	Stefan Boltzmann constant = $1.365 \times 10^{-12} \text{ cal/sec cm}^2 (^\circ\text{K})^4$



## NOMENCLATURE (Cont'd)

### Subscripts

<i>a</i>	actual value from calculation
<i>c</i>	core
<i>l</i>	hydrogen in the liquid state at 20°K
max	maximum value
<i>N</i>	<i>N</i> th (maximum-temperature) zone of hydrogen
<i>n</i>	<i>n</i> th zone of hydrogen ( $1 \leq n \leq N$ )
net	net value
<i>p</i>	propellant (hydrogen)
<i>p,c</i>	propellant in cavity
<i>r</i>	reflector and radius to inner reflector surface
<i>s</i>	seed material (tantalum carbide)
<i>T<sub>r</sub></i>	evaluated at peak reflector temperature
<i>T<sub>N</sub></i>	evaluated at maximum hydrogen temperature

### Superscript

<i>T</i>	property evaluated at appropriate temperature (e.g., $T_n$ , $T_c$ , etc.)
----------	--

## II. CRITICALITY ANALYSIS

The results of the preceding analysis indicate that substantial thicknesses of hydrogen are required to absorb the thermal energy emanating from the core. Reflection of this effect on criticality is the subject of Part II.

The criticality of a cavity reactor system has been treated by Safonov (Ref. 7) for the moderator and fuel at room temperature. This technique was utilized in Ref. 1 to determine critical concentration versus core radius for a high-temperature ( $2000^{\circ}\text{K}$ ) moderator. However, in both analyses, contact of the core and reflector surfaces was assumed; i.e.,  $r_c = r_r$ .

This analysis investigates the effect of an intervening void (the propellant) on reactor criticality. The reactor is composed of three regions, as shown in Fig. 6. The three regions are core, pure fissionable material, the void (space occupied by the propellant), and the reflector-moderator (graphite).

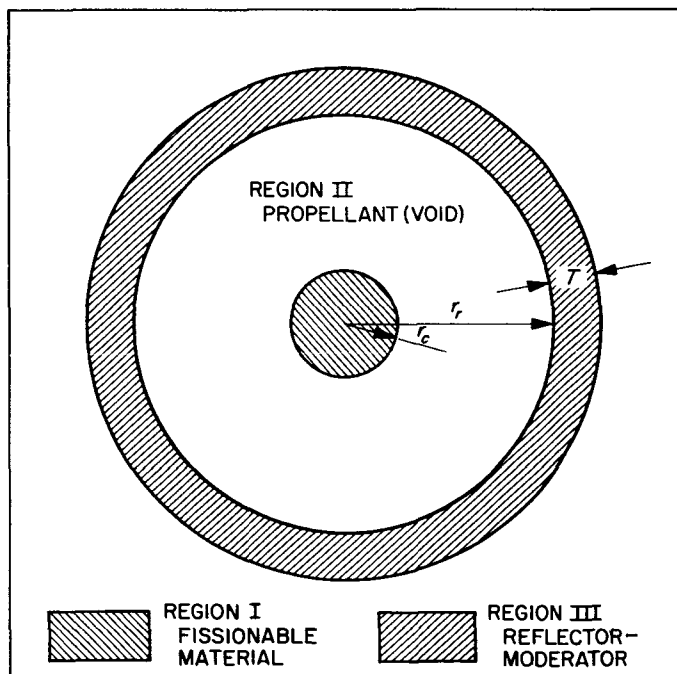


Fig. 6. The three regions of a gaseous core reactor

Two-group diffusion theory is utilized to determine the fast and thermal flux distributions in the reflector, subject to continuity of fast and slow currents at the inner reflector surface and an extrapolated flux boundary condition at the exterior moderator surface on the fast and slow fluxes.

The reactor criticality thus resolves itself into a two-group, single-region problem with the use of appropriate boundary conditions.

The following simplifying assumptions have been made in the analysis:

1. Diffusion theory is applicable to the reflector. (This approximation should be applicable for reflector thicknesses  $\geq 1$  m.)
2. The reflector has a uniform temperature of 2500°K. Its microscopic-absorption cross section has its room-temperature value (for conservatism).
3. The flow of neutrons toward the core at the inner reflector surface has a cosine distribution peaked in the forward direction.
4. The intervening layer of propellant is treated as a void (a good assumption, since the transport mean free path in hydrogen at 30 atm is approximately 60 m).
5. The core proper does not scatter neutrons; it simply absorbs thermal neutrons.
6. The reactor has spherical symmetry.
7. The extrapolation distance is the same for fast or thermal neutrons leaving the reflector.

The two-group diffusion equations which must be solved in the reflector are:

$$D_{1,r} \nabla^2 \phi_{1,r} - \Sigma_{1,r} \phi_{1,r} = 0 \quad (20)$$

$$D_{2,r} \nabla^2 \phi_{2,r} - \Sigma_{2,r} \phi_{2,r} + \Sigma_{1,r} \phi_{1,r} = 0 \quad (21)$$

The fast flux equation is homogeneous and may be solved directly.

$$\phi_{1,r} = \frac{C_1}{r} \sinh K_{1,r} r + \frac{C_2}{r} \cosh K_{1,r} r \quad (22)$$

where

$$K_{1,r}^2 = \frac{\Sigma_{1,r}}{D_{1,r}} \quad (23)$$

Application of the extrapolation-length boundary condition at the exterior of the reflector

$$\phi_{1,r} = 0 \qquad r = r_r + a \qquad (24)$$

where

$$a = T_r + (\lambda_{tr})_r \qquad (25)$$

yields

$$\phi_{1,r} = \frac{C \sinh K_{1,r} (r_r + a - r)}{r} \qquad (26)$$

where

$$C = - \frac{C_1}{\cosh K_{1,r} (r_r + a)} \qquad (27)$$

The second boundary condition on  $\phi_{1,r}$  is dependent on the number of fast neutrons/sec entering the reflector from the core. The fast-neutron current entering the reflector is, of course, dependent on the average thermal-neutron flux in the core, which, in turn, depends on the net thermal-neutron current into the core from the reflector. This neutron balance provides the basis for obtaining a critical reactor equation and the attendant flux distributions in the reflector.

The number of neutrons produced per second in the core is

$$I_{1,c} = \nu \Sigma_{f,c} \bar{\phi}_{2,c} V_c \qquad (28)$$

and the net current density at the surface of the core is

$$(J_1)_{r_c}^{\text{net}} = \frac{\nu \Sigma_{f,c} \bar{\phi}_{2,c} V_c}{A_c} \qquad (29)$$

From continuity of current, the current density at the inner surface of the reflector must be

$$(J_1)_{r_r}^{\text{net}} = \frac{\nu \Sigma_{f,c} \bar{\phi}_{2,c} V_c}{A_{r_r}} \quad (30)$$

The net number of thermal neutrons absorbed per second in the core is

$$I_{2,c} = \Sigma_{a,c} \bar{\phi}_{2,c} V_c \quad (31)$$

and the required thermal-neutron surface-current density inward is

$$(J_2)_{r_c}^{\text{net}} = - \frac{\Sigma_{a,c} \bar{\phi}_{2,c} V_c}{A_c} \quad (32)$$

From continuity of current

$$(J_2)_{r_r}^{\text{net}} = - \frac{\Sigma_{a,c} \bar{\phi}_{2,c} V_c}{A_{r_r}} \quad (33)$$

By combining Eqs. (30) and (33),

$$(J_1)_{r_r}^{\text{net}} = - (J_2)_{r_r}^{\text{net}} \nu \left( \frac{\Sigma_{f,c}}{\Sigma_{a,c}} \right) \quad (34)$$

or

$$\boxed{(J_1)_{r_r}^{\text{net}} = - \eta (J_2)_{r_r}^{\text{net}}} \quad (35)$$

Equation (35) represents the second boundary condition on  $\phi_{1,r}$  which must be satisfied. Since the thermal-flux distribution in the reflector is unknown, we must delay the final solution to Eq. (26).

The solution of Eq. (21) involves the sum of a complementary and particular integral. Substituting Eq. (26) into (21),

$$D_{2,r} \left( \frac{\partial^2 \phi_{2,r}}{\partial r^2} + \frac{2}{r} \frac{\partial \phi_{2,r}}{\partial r} \right) - \Sigma_{2,r} \phi_{1,r} + \Sigma_{1,r} \frac{C \sinh K_{1,r} (r_r + a - r)}{r} = 0 \quad (36)$$

The complementary solution of Eq. (36), after applying the extrapolation-distance boundary condition and assumption 7, has the form of Eq. (26):

$$\phi_{2,r} (\text{comp}) = \frac{B \sinh K_{2,r} (r_r + a - r)}{r} \quad (37)$$

where

$$K_{2,r}^2 = \frac{\Sigma_{2,r}}{D_{2,r}} \quad (38)$$

The particular integral may be obtained by the method of undetermined coefficient. The general solution is then

$$\phi_{2,r} = \frac{B \sinh K_{2,r} (r_r + a - r)}{r} - \frac{\frac{\Sigma_{1,r}}{D_{2,r}}}{K_{1,r}^2 - K_{2,r}^2} \frac{C \sinh K_{1,r} (r_r + a - r)}{r} \quad (39)$$

In order to evaluate the two arbitrary constants, an additional relationship to Eq. (35) is required.

As mentioned previously, the reflector supplies the thermal neutrons which are absorbed in the core. However the core does not absorb all thermal neutrons entering the cavity, (1) because of the relative geometry of core and reflector and (2) because the core is not necessarily completely "opaque" to thermal neutrons. Thus, in general, there is a probability of capture in the core which is less than one. Let this probability be  $P$ .

Those thermal neutrons which are not absorbed by the core make up the outgoing thermal current at the wall.

This is the only thermal current outward at the wall, since it has been assumed that no thermal neutrons are born or arise in the core. Mathematically, this may be stated by

$$(J_2)_{r_r}^+ = (1 - P) (J_2)_{r_r}^- \quad (40)$$

and

$$(J_2)_{r_r}^{\text{net}} = (J_2)_{r_r}^+ - (J_2)_{r_r}^- \quad (41)$$

or

$$\boxed{(J_2)_{r_r}^{\text{net}} = - P (J_2)_{r_r}^-} \quad (42)$$

Equation (42) is the second boundary condition to be used in evaluating one of the remaining arbitrary constants and obtaining a critical condition. The second arbitrary constant is, of course, set by the reactor power level. Application of Eqs. (35) and (42) to Eqs. (26) and (39) is made in Appendix B. The utilization of these two conditions allows one to obtain an explicit form for the probability  $P$ , independent of the fuel concentration in the core. From Appendix B, Eq. (B-15),

$$P = \frac{1 + K_{2,r} r_r \coth K_{2,r} a}{\frac{K_{1,r}^2}{K_{1,r}^2 - K_{2,r}^2} \frac{\eta r_r}{4D_{2,r}} \frac{K_{1,r} r_r \cosh K_{1,r} a - K_{2,r} r_r \sinh K_{1,r} a \coth K_{2,r} a}{\sinh K_{1,r} a + K_{1,r} r_r \cosh K_{1,r} a} - \frac{r_r - 2D_{2,r} (1 + K_{2,r} \coth K_{2,r} a)}{4D_{2,r}}} \quad (43)$$

Let us call this  $P$  the geometric probability  $P_g$ , in analogy to the geometric buckling. This probability must be equal to the "material" probability  $P_m$ , which is dependent on the probability of capture in the core. Thus, the critical condition for such a system has the form

$$P_g = P_m \quad (44)$$

As yet, the form of  $P_m$  has not been stipulated; however, it must depend on the ability of the core to capture thermal neutrons. Now, from assumption 5, the probability of penetrating the core along any path is

$$z = e^{-N_c \sigma_{a,c} l_c(\theta)} \quad (45)$$

and the probability of capture is

$$(1 - z) = 1 - e^{-N_c \sigma_{a,c} l_c(\theta)} \quad (46)$$

The path length traveled by a particular neutron penetrating the core is dependent on the relative orientation of the reflector wall and core, as shown in Fig. 7. From geometry,

$$l_p = r_c \cos \alpha + r_r \cos \theta \quad (47)$$

$$(90^\circ \leq \alpha \leq 180^\circ)$$

$$\sin \beta = \frac{r_r}{r_c} \sin \theta \quad (48)$$

$$(0 \leq \beta \leq 90^\circ)$$

$$l_T = l_p + l_c = r_c \cos \beta + r_r \cos \theta \quad (49)$$

But,

$$\beta = 180^\circ - \alpha \quad (50)$$

$$l_c(\theta) = l_T - l_p = -2r_c \cos \alpha \quad (51)$$

and

$$\sin \alpha = \frac{r_r}{r_c} \sin \theta \quad (52)$$



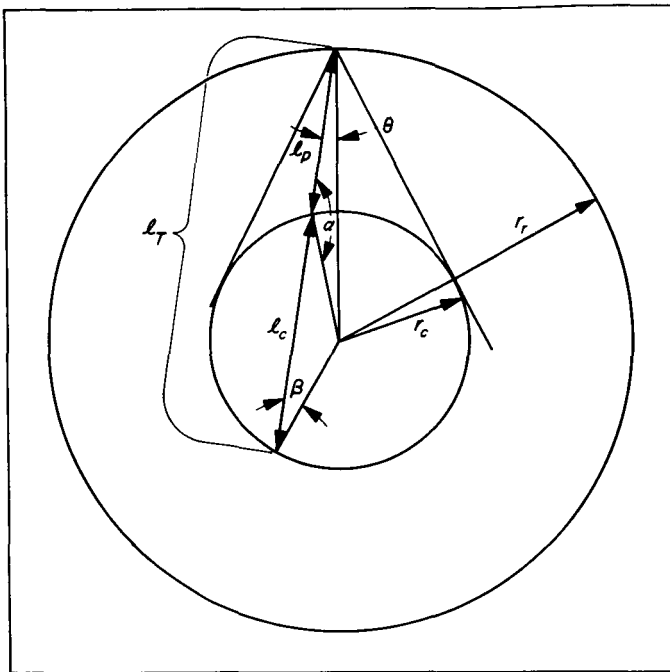


Fig. 7. Geometric path length of neutron penetrating the core

Equation (51) is valid to  $\sin \theta_{\max}$ , which is given by

$$\sin \theta_{\max} = \frac{r_c}{r_r} \quad (53)$$

Equation (51) gives the desired form for the neutron path length as a function of  $\theta$ , the angle of departure from the vertical at the wall. The distribution of neutrons leaving the wall is assumed to be a cosine, peaked in the forward direction (assumption 3). Then, the total probability of capture in the core  $P_m$ , after appropriate normalization, is

$$P_m = \frac{1}{\pi} \int_0^{\theta_{\max}} \cos \theta \, 2\pi \sin \theta \, [e^{-\Sigma_{a,c} l_c(\theta)}] \, d\theta \quad (54)$$

since

$$N_c \sigma_{a,c} = \Sigma_{a,c} \quad (55)$$

The integration of Eq. (54) is carried out in Appendix C. The final form for  $P_m$  (Eq. C-9) is

$$P_m = \sin^2 \theta_{\max} \left\{ 1 + \frac{2}{(2\Sigma_{a,c} r_c)^2} \left[ e^{-2\Sigma_{a,c} r_c (2\Sigma_{a,c} r_c + 1)} - 1 \right] \right\} \quad (56)$$

Solution of Eq. (56) consistent with Eq. (43) determines the critical concentration in the core.

Once the critical concentration has been determined for a given configuration, the flux distribution in the reflector can be determined as a function of the average thermal flux in the core. This is carried out in Appendix D, and the results are given below:

$$\frac{\phi_{1,r}}{\phi_{2,c}} = \frac{\nu \Sigma_f r_c^3}{3D_1} \frac{1}{\sinh K_{1,r} a + K_{1,r} r_r \cosh K_{1,r} a} \frac{\sinh K_{1,r} (r_r + a - r)}{r} \quad (57)$$

$$\frac{\phi_{2,r}}{\phi_{2,c}} = \frac{\nu \Sigma_f r_c^3}{3D_1} \left[ \left( \frac{\Sigma_{1,r}}{D_{2,r}} - \frac{D_{1,r}}{\eta D_{2,r}} \right) \frac{1}{r} \frac{\sinh K_{2,r} (r_r + a + r)}{\sinh K_{2,r} a + K_{2,r} r_r \cosh K_{2,r} a} - \frac{\Sigma_{1,r}}{D_{2,r}} \frac{1}{r} \frac{\sinh K_{1,r} (r_r + a - r)}{\sinh K_{1,r} a + K_{1,r} r_r \cosh K_{1,r} a} \right] \quad (58)$$

The critical concentration of plutonium as a function of  $r_c/r_r$  and core radius for reflector thicknesses of 100 and 200 cm is given in Figs. 8 and 9. The nuclear constants used in this analysis are tabulated in Appendix E. For comparison, data from Ref. 1, based on the analysis of Safonov (Ref. 7) are given in Fig. 8 for a reflector thickness of 100 cm and  $r_c/r_r = 1.0$ . The two-group theory is within 20% of the more sophisticated theory in all cases, thus substantiating its applicability. The most important result is the sharp increase in critical concentration required for ratios of  $r_c/r_r < 0.5$ . This effect arises principally from the fact that even though the core is opaque to thermal neutrons, it is very difficult for them to "find" the core.

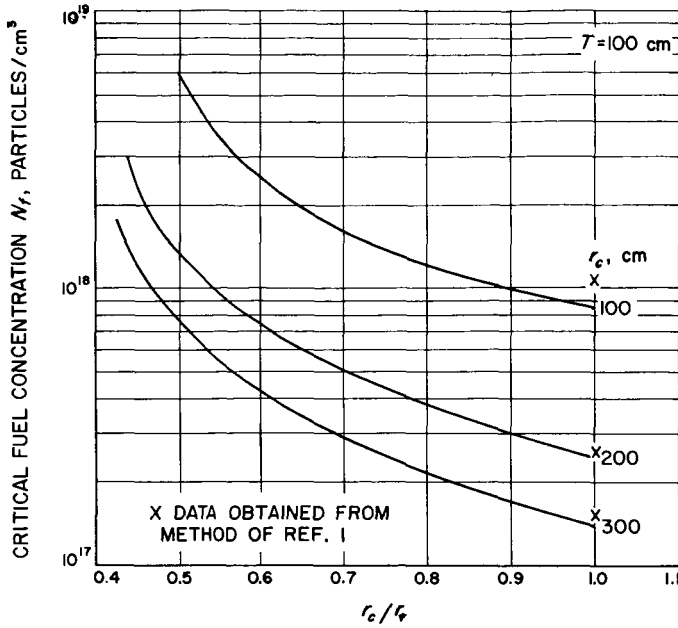
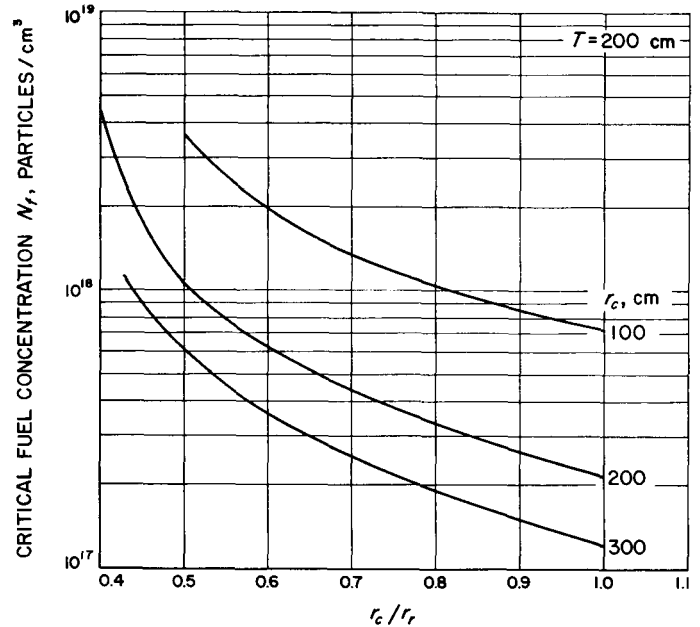


Fig. 8. Critical fuel concentration vs  $r_c/r_r$  for  $T = 100$  cm

Fig. 9. Critical fuel concentration vs  $r_c/r_r$  for  $T = 200$  cm



Comparison of Figs. 8 and 9 shows the effect of reflector thickness on reactor criticality. The critical concentration decreases somewhat with the thicker reflector; however, the asymptotic value of  $r_c/r_r$  does not change appreciably. For reflector thicknesses greater than 200 cm, there is effectively no reduction in critical concentration. This arises from the fact that although the leakage decreases, the capture within the graphite is increasing.

Figures 10 and 11 show the critical masses associated with Figs. 8 and 9, respectively. Of course, the critical mass depends on the reflector thickness in the same way as the critical concentration. From a criticality standpoint, the 200-cm-thick reflector is desirable; however, the reflector weight is twice as great as that of the 100-cm one.

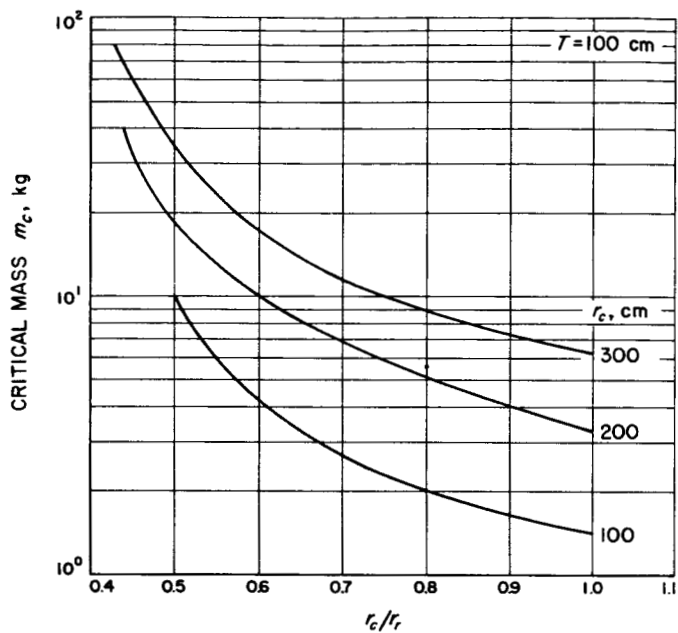


Fig. 10. Critical mass vs  $r_c/r_r$  for  $T = 100$  cm

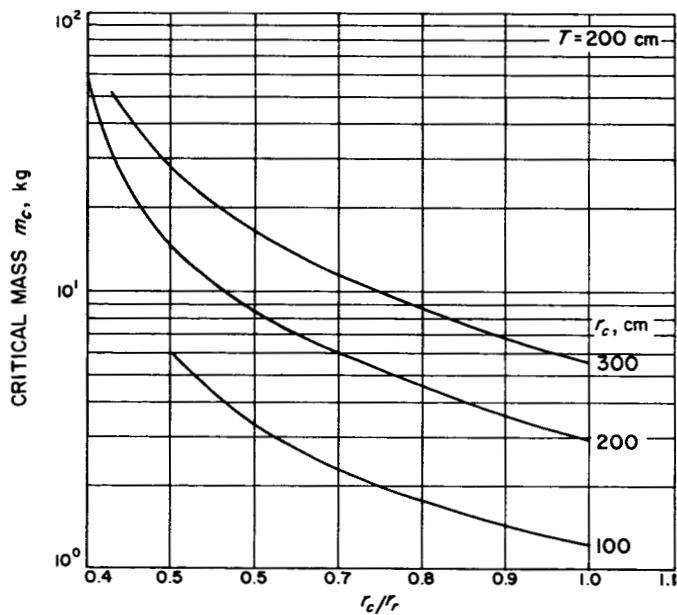


Fig. 11. Critical mass vs  $r_c/r_r$  for  $T = 200$  cm

Typical fast- and thermal-flux distributions are shown in Figs. 12-14. The sharp peaking of the thermal-neutron flux near the interior wall is characteristic of the externally moderated reactors.

Fig. 12. Flux distribution in reflector  
 ( $r_c = 300$  cm,  $r_r = 500$  cm,  $T = 100$  cm)

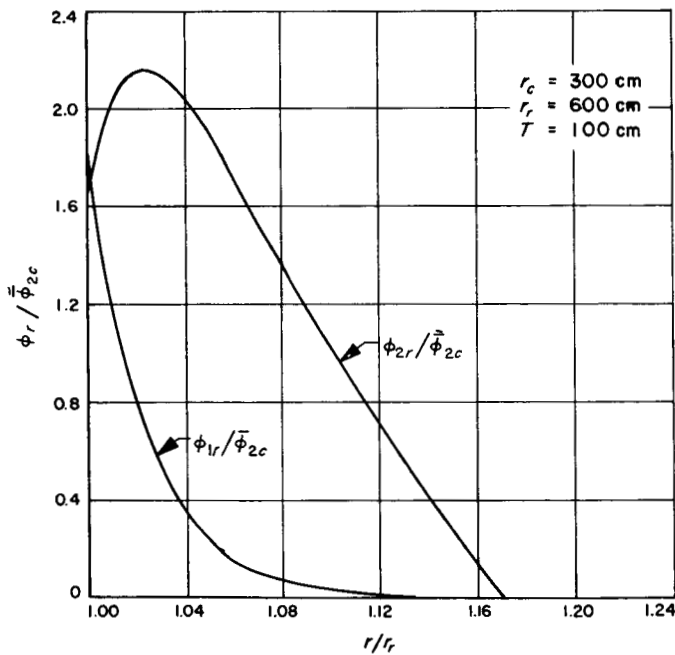
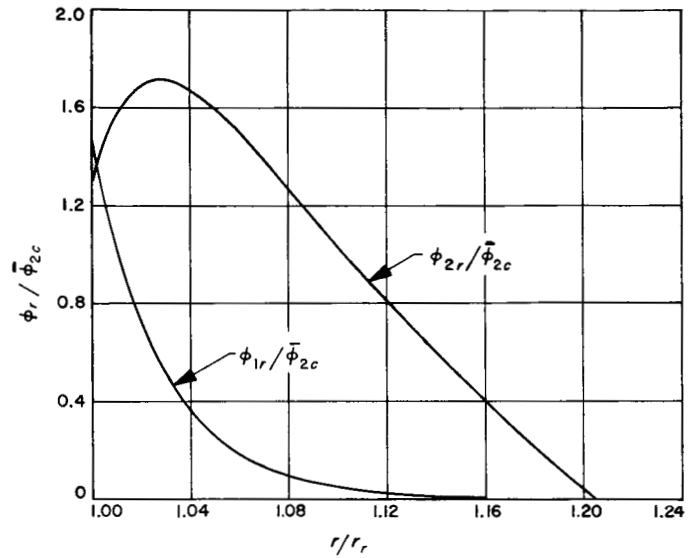
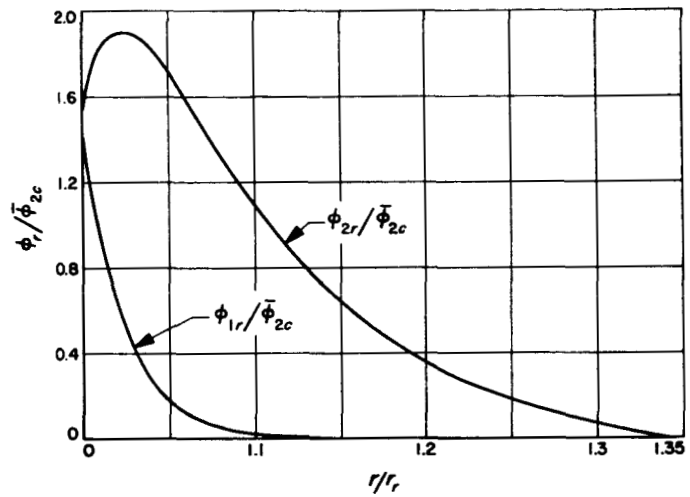


Fig. 13. Flux distribution in reflector  
 ( $r_c = 300$  cm,  $r_r = 600$  cm,  $T = 100$  cm)

Fig. 14. Flux distribution in reflector  
 ( $r_c = 300$  cm,  $r_r = 600$  cm,  $T = 200$  cm)



Comparison of Figs. 12 and 13 shows the effect of a larger hydrogen thickness on the reflector flux distribution as  $r_c/r_r$  increases. Since it is more difficult for the thermal neutrons to “find” the core with the thicker hydrogen zone, the thermal-flux peaking in the reflector is more pronounced.

Comparison of Figs. 13 and 14 indicates the effect of increasing the reflector thickness. The fast-flux distributions do not change appreciably, but the peaking of the thermal flux is less pronounced for the thicker reflector. This is, of course, due to the lower neutron leakage in this case.

## NOMENCLATURE

(Part II and Appendixes B, C, D, and E)

$A$	surface area, $\text{cm}^2$
$a$	reflector thickness plus extrapolation distance, cm
$B$	arbitrary constant, neutrons/cm sec
$C, C_1, C_2$	arbitrary constants, neutrons/cm sec
$D$	diffusion coefficient, cm
$l$	number of neutrons produced, neutrons/sec
$J$	neutron current density, neutrons/ $\text{cm}^2$ sec
$l$	neutron path length, cm
$N$	particle concentration, particles/ $\text{cm}^3$
$P$	probability of capture
$r$	radial coordinate, cm
$T$	reflector thickness, cm
$V$	volume, $\text{cm}^3$
$x$	dimensionless parameter
$z$	probability of penetrating core
$\alpha$	exterior angle in Fig. 8 related to $\theta$ , rad
$\beta$	interior angle in Fig. 8 related to $\theta$ , rad
$\eta$	number of neutrons produced per absorption
$\theta$	angle from local vertical to direction of motion of the neutron, rad
$K$	inverse diffusion length, $\text{cm}^{-1}$
$\lambda$	mean free path, cm
$\nu$	average number of neutrons produced per fission
$\xi$	dimensionless parameter
$\Sigma_c$	macroscopic cross section in core, $\text{cm}^{-1}$

$\Sigma_r$	macroscopic removal cross section in reflector, $\text{cm}^{-1}$
$\sigma$	microscopic cross section, barns
$\phi$	neutron flux, neutrons/ $\text{cm}^2 \text{ sec}$
$\tau$	neutron age, $\text{cm}^2$
$\nabla^2$	Laplacian operator in spherical coordinates, $\text{cm}^{-2}$

**Subscripts**

<i>a</i>	absorption
<i>c</i>	core
<i>f</i>	fission
<i>g</i>	geometric
<i>m</i>	material
max	maximum value
<i>p</i>	propellant
<i>r</i>	reflector and radius to inner reflector surface
<i>T</i>	total
<i>tr</i>	transport property
1	fast neutrons
2	thermal neutrons

**Superscripts**

net	net value
<i>r</i>	reflector
+	directed outward
-	directed inward
29	plutonium 239



### III. SUPERPOSITION OF RESULTS FROM PARTS I AND II

The effect of superimposing the restrictions imposed in Parts I and II are now considered. Basically, the thermal analysis specifies the thickness of hydrogen required to heat the propellant to a certain temperature. This, in turn, determines the operating-engine specific impulse. The criticality analysis, on the other hand, indicates the ratio of core to inner reflector radius necessary to obtain a critical system for a particular core radius. Both analyses, therefore, are dependent on the thickness of hydrogen, which is the required link between the solutions.

If the asymptotic value of core-to-wall radius is assumed for a particular core radius, the maximum achievable specific impulse for the system can be determined (Fig. 15). The cross-hatched region to the right of the curve indicates the theoretical operating conditions for the engine, assuming a reflector thickness of 100 cm. For example, to achieve an engine specific impulse of 2000 sec, the core radius must be at least 220 cm. Since the reflector weight increases for a given thickness of propellant as the core radius increases, operation as near the limiting curve as possible is desirable from a performance standpoint.

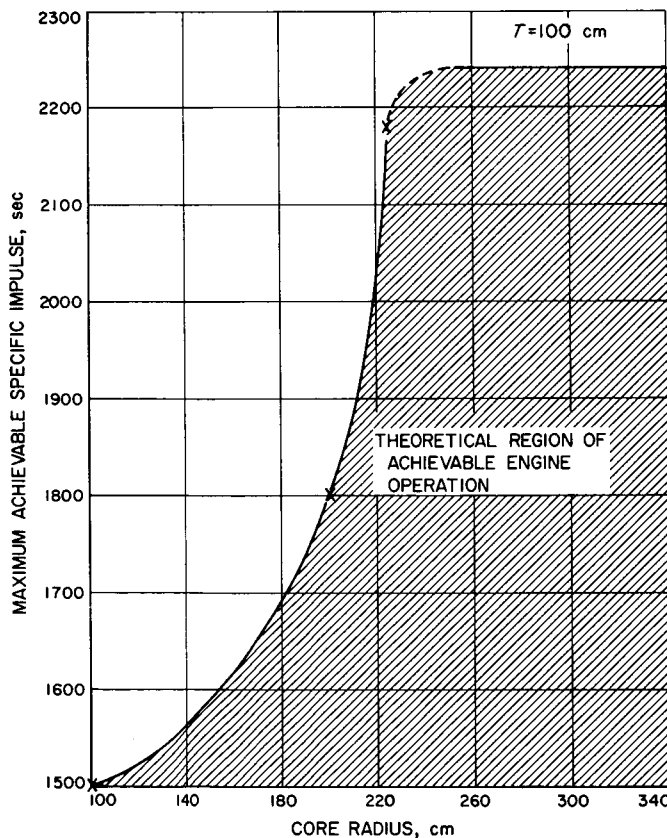


Fig. 15. Maximum achievable engine specific impulse based on thermal and criticality constraints ( $T_c \geq 20,000^\circ\text{K}$ )

As the asymptotic ratio of core to inner reflector radius was assumed in Fig. 15, the required critical mass is infinite for all cases falling on the curve. Practical operation, therefore, requires a core radius which lies within the cross-hatched region.

Figure 16 presents the engine thrust as a function of core radius and core temperature. The core temperature is limited to a value greater than 20,000°K, because this was the applicable region for the simplified thermal analysis. Although operation at lower core temperatures is possible, a loss in engine specific impulse and performance will occur. Preliminary weight estimates also indicate that for lower thrust levels, the engine thrust-to-weight ratio is less than 1.0.

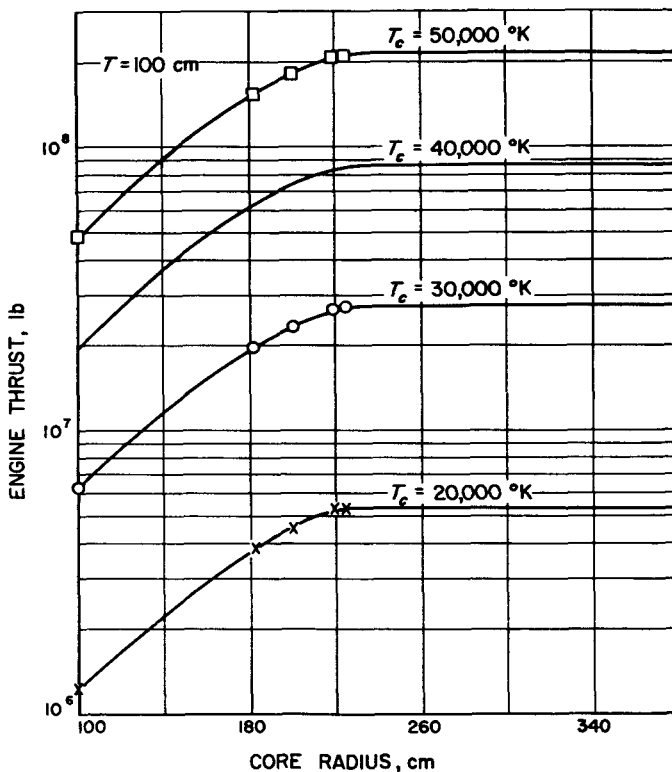


Fig. 16. Achievable engine thrust based on thermal and criticality constraints (T<sub>c</sub> ≥ 20,000°K)

As was stated in Ref. 1, the minimum engine thrust level is approximately 10<sup>6</sup> lb, and higher values are easily attained by increasing the core temperature. The achievable thrust, thus, lies above the curve shown for T<sub>c</sub> = 20,000°K for near-maximum performance.

As examples of engine characteristics, a specific impulse of approximately 1550 sec at an engine thrust of 2 × 10<sup>6</sup> lb, or a specific impulse of approximately 2200 sec at a thrust of 5.3 × 10<sup>6</sup> lb, is achievable. The performance of vehicle systems with these characteristics, including weight breakdowns, will be the subject of a subsequent Report by the author.

## **ACKNOWLEDGEMENT**

The author is grateful to Dr. Clifford J. Heindl of the JPL Physics Section for helpful discussions regarding the criticality problem and to Mrs. Carolyn Level, who performed the numerical calculations in Part II.

## REFERENCES

1. Spencer, D. F., *The Plasma Core Reactor*, Technical Report No. 32-104, Jet Propulsion Laboratory, Pasadena, California, April 24, 1961.
2. Weinstein, H. and Ragsdale, R. G., *A Coaxial Flow Reactor—A Gaseous Nuclear-Rocket Concept*, Lewis Research Center. Presented at the ARS 15th Annual Meeting, Shoreham Hotel, Washington, D. C., Dec. 5-8, 1960.
3. Meghreblian, R. V., *Gaseous Fission Reactor for Spacecraft Propulsion*, Technical Report No. 32-42, Jet Propulsion Laboratory, Pasadena, California, July 6, 1960.
4. Olfe, D., *Equilibrium Emissivity Calculations for a Hydrogen Plasma at Temperatures up to 10,000° K*, Technical Report No. 33, Guggenheim Aeronautical Laboratory, California Institute of Technology, Pasadena, California, May, 1960.
5. Barre, J. J., *Essai de Contribution à l'Autopropulsion Nucléaire*, Presented at the VIIIth International Astronautical Congress, Barcelona, 1957.
6. Altman, D., *Thermodynamic Properties and Calculated Rocket Performance of Hydrogen to 10,000° K*, Report No. 20-106, Jet Propulsion Laboratory, Pasadena, California, September 3, 1956.
7. Safonov, G., "Externally Moderated Reactors," *Second United Nations International Conference on the Peaceful Uses of Atomic Energy*, Vol. 12, 1958, p. 705.
8. Hughes, D. J., and Schwartz, R. B., *Neutron Cross Sections*, BNL 325, Brookhaven National Laboratory, Upton, New York, 2nd edition, July 1, 1958.

## APPENDIX A

### Calculation of Temperature Distribution in the Propellant

The utilization of Eqs. (5) and (7) to obtain the temperature profile and hydrogen-layer thickness requires an estimate of the propellant flow rate which is to be used. To obtain this estimate,  $\delta_{th}$  is assumed to be zero. Then,

$$\frac{\Delta H_{p,c}}{\Delta H_r} = \frac{1 - \delta_N}{\delta_N} \quad (A-1)$$

For booster applications (i.e., short reactor operating times), the nuclear energy deposited directly in the reflector is approximately 7% of the total reactor power; therefore,  $\delta_N$  is assumed to be 0.07 in this analysis. For a peak moderator-reflector temperature of 2500°K,  $\Delta H_r = 9.65 \times 10^3$  cal/g atom for a hydrogen pressure of 30 atm.

Then,

$$\Delta H_{p,c} = 1.29 \times 10^5 \text{ cal/g}$$

$$T_N = (T_p)_{\max} = 13,300^\circ \text{K}$$

Since it has been assumed that all the thermal energy is absorbed in the propellant,

$$\dot{w}_p \Delta H_{p,c} \simeq \sigma A_c (T_c^4 - T_N^4) \quad (A-2)$$

For a typical core temperature of 30,000°K and a core radius of 1 m,

$$\dot{w}_p = 1.06 \times 10^6 \text{ g/sec } (2.33 \times 10^3 \text{ lb/sec})$$

This represents the minimum flow rate required in the reflector, since there will be some thermal transfer to the reflector. The other extreme is simply the case in which all the thermal energy reaches the reflector. Then,

$$\dot{w}_p = 1.44 \times 10^7 \text{ g/sec } (3.17 \times 10^4 \text{ lb/sec})$$

In obtaining the stepwise solution to Eq. (7), the value of  $\epsilon/L$  is taken from Fig. 1 at  $T_{n-1}$ ; i.e., the low-temperature value is utilized for conservatism. The  $\Delta T$  for a particular zone is assumed, and the thickness required to produce this  $\Delta T$  is calculated. Small increments in  $\Delta T$  are taken when the propellant emissivity is low and larger  $\Delta T$  when the emissivity is higher.

By assuming various flow rates and peak temperatures, calculating stepwise the  $\Delta r$  required per zone, then calculating  $(\delta_{th})_a$  from the stepwise process, and finally comparing it with the required  $\delta_{th}$  for the assumed  $(T_p)_{\max}$ , the maximum obtainable hydrogen temperature is determined for a particular flow rate.

A sample calculation is given below for a core temperature of 30,000°K, a core radius of 100 cm, a flow rate of  $1.36 \times 10^6$  g/sec (3000 lb/sec), and an assumed peak hydrogen temperature of 11,000°K:

$$Q_n = \dot{w}_p \Delta H_n = 1.36 \times 10^6 \Delta H_n$$

The first increment in  $\Delta T$  is assumed to be from 10,000 to 11,000°K; then,  $\bar{T}_N = 10,500^\circ\text{K}$ ;  $\Delta H_N = 7.5 \times 10^3$  cal/g, and we have

$$1.02 \times 10^{10} = (1.365 \times 10^{-12}) (4\pi \times 10^4) (\epsilon/L)_N \Delta r_N [(3 \times 10^4)^4 - (1.05 \times 10^4)^4] \\ - 4\pi (100 + \Delta r_N)^2 (\epsilon/L)_N \Delta r_N (1.05 \times 10^4)^4$$

$$(\epsilon/L)_{10,000^\circ\text{K}} = 6.5 \times 10^{-2}/\text{cm}$$

By neglecting the second-order term in  $\Delta r$ ,

$$\Delta r_N = 1.2 \text{ cm}$$

and

$$\alpha_N = 0.076 \qquad 1 - \alpha_N = 0.924$$

since  $\Delta r \ll r$ , second-order terms are negligible and no iteration is required. For the  $N-1$  zone,  $\Delta T$  from 8000 to 10,000°K,  $\Delta H_{N-1} = 12 \times 10^3$  cal/g,

$$Q_{N-1} = 1.64 \times 10^{10} = (1.72 \times 10^{-7}) \left( \frac{\epsilon}{L} \right)_{N-1} \Delta r_{N-1} (0.924) [(3 \times 10^4)^4 - \text{negligible} \\ - (0.9 \times 10^4)^4] + \text{negligible} - (1.76 \times 10^{-7}) \left( \frac{\epsilon}{L} \right)_{N-1} \Delta r_{N-1} (0.9 \times 10^4)^4$$

where  $\epsilon/L = 9 \times 10^{-3}$ /cm. Then,

$$\Delta r_{N-1} = 14.5 \text{ cm}$$

and

$$\alpha_{N-1} = 0.130 \qquad 1 - \alpha_{N-1} = 0.870$$

Again, since the dominant term is simply the plasma emission, no iteration is necessary.

In a similar manner, the remaining  $\Delta r$  (except  $\Delta r_1$ ) were obtained. These are shown in Table A-1.

The determination of  $\Delta r_1$ , as explained in Part I, depends on the photon wavelength at the peak of the black-body radiation curve for a core temperature of 30,000°K:

$$\lambda_{T_c} = \frac{0.293}{30,000} \simeq 0.1 \mu = 10^{-5} \text{ cm}$$

The minimum practical TaC particle size which can be obtained has a diameter of  $0.1 \mu$ . From Fig. 4 of Ref. 5 and  $r_s/\lambda = 0.5$ ,  $K = 10$ . For a peak hydrogen temperature of 11,000°K at 30 atm,

$$\rho_p \simeq 6.7 \times 10^{-5} \text{ g/cm}^3$$

$$\rho_s = 14.65 \text{ g/cm}^3$$

Table A-1. Determination of  $\Delta r_n$  and  $\alpha_n$

$\Delta T_n$ °K	$(\epsilon/L)_n$ cm <sup>-1</sup>	$\Delta H_n$ 10 <sup>3</sup> cal/g	$\Delta r_n$ cm	$\alpha_n$ dimensionless	$n$ dimensionless
10,000 - 11,000	$6.5 \times 10^{-2}$	7.5	1.2	0.076	11
8,000 - 10,000	$9.0 \times 10^{-3}$	12	14.1	0.13	10
7,500 - 8,000	$5.6 \times 10^{-3}$	3.5	7.6	0.042	9
7,000 - 7,500	$3.0 \times 10^{-3}$	3.5	14.8	0.044	8
6,800 - 7,000	$2.4 \times 10^{-3}$	2.0	11.0	0.026	7
6,600 - 6,800	$1.9 \times 10^{-3}$	2.0	14.3	0.027	6
6,400 - 6,600	$1.3 \times 10^{-3}$	2.0	21.6	0.028	5
6,200 - 6,400	$1.0 \times 10^{-3}$	2.5	36.1	0.036	4
6,000 - 6,200	$7 \times 10^{-4}$	2.5	53.4	0.037	3
5,800 - 6,000	$5 \times 10^{-4}$	3	93.4	0.047	2
2,500 - 5,800		61		0.994	1

Since  $\alpha_1 = 0.994$ ,  $Q_n/Q_1 = 0.006$ , and  $\ln Q_1/Q_r = 5.1$ . Then, substituting into Eq. (17),

$$\Delta r_1 = 37.4 \text{ cm}$$

and

$$r_r - r_c = \sum_{n=1}^N \Delta r_n$$

Then,

$$r_r - r_c = 305 \text{ cm}$$

Now,

$$(\delta_{th})_a = \frac{(0.006) (0.65) (1.29 \times 10^{11})}{1.39 \times 10^{11}} = 0.0036$$



In a similar manner, other values of  $r_r - r_c$  and  $(\delta_{th})_a$  can be determined by assuming various values of  $T_N$ . These are plotted on curves 1 and 2, respectively, in Fig. 3. The required maximum hydrogen temperature for various values of  $\delta_{th}$  are given in Table A-2 and shown as curve 3 in Fig. 3. The intersection of curves 2 and 3 gives the consistent value of  $(T_h)_{max}$ , and a horizontal line drawn to intersect curve 1 sets the required hydrogen thickness.

Table A-2. Enthalpy rise and maximum propellant temperature

$\delta_{th}$ dimensionless	$\Delta H_{p,c}$ $10^3$ cal/g	$T_N$ °K
0	128.5	13,300
0.001	126.6	13,200
0.005	119.8	12,700
0.01	112.1	12,100
0.02	99.3	10,800
0.03	88.9	9,200
0.04	80.4	8,000
0.06	67.1	6,200
0.07	61.8	5,800

Although the results presented in Fig. 4 were calculated for a core radius of 100 cm, they are, to within calculational accuracy, independent of  $r_c$ . This stems from the fact that the major heating contribution to each hydrogen zone results from the direct interchange with the core. Increasing the core radius by some multiple increases the heat rejected by the core by the square of this multiple. Since the enthalpy rise per zone for a given  $\Delta T_m$  is fixed, this merely requires an increase in flow rate by a factor of the multiple squared to obtain a new operating condition. As a result, neither  $r_r - r_c$  nor  $T_n$  is changed; thus, these results are valid for any core radius.

A similar argument can be used in determining the effect of core temperature. Since back emission from the hydrogen contributes very little at core temperatures above 20,000°K, the hydrogen thickness required and maximum hydrogen temperature are independent of the core temperature to calculational accuracy.

In this case, however, the flow rate increases as the fourth power of the multiple increase in the core temperature. Thus, Fig. 4 presents results which are independent of the core radius and temperature but which are dependent on the propellant flow rate or, in other words, engine thrust.

APPENDIX B

Application of Continuity Conditions on Thermal and Fast Currents

The thermal- and fast-flux equations in the reflector are

$$\phi_{2,r} = \frac{B \sinh K_{2,r} (r_r + a - r)}{r} - C \frac{\frac{\Sigma_{1,r}}{D_{2,r}} \sinh K_{1,r} (r_r + a - r)}{K_{1,r}^2 - K_{2,r}^2} \quad (B-1)$$

and

$$\phi_{1,r} = \frac{C \sinh K_{1,r} (r_r + a - r)}{r} \quad (B-2)$$

where

$$C = - \frac{C_1}{\cosh K_{1,r} (r_r + a)} \quad (B-3)$$

The boundary conditions to be applied are

$$(J_1)_{r_r}^{\text{net}} = - \eta (J_2)_{r_r}^{\text{net}} \quad (B-4)$$

$$(J_2)_{r_r}^{\text{net}} = - P (J_2)_{r_r}^- \quad (B-5)$$

Now,

$$(J_1)_{r_r}^{\text{net}} = - D_{1,r} \left( \frac{\partial \phi_{1,r}}{\partial r} \right)_{r_r} = D_{1,r} C \frac{\sinh K_{1,r} a + K_{1,r} r_r \cosh K_{1,r} a}{r_r^2} \quad (B-6)$$

$$(J_2)_{r,r}^{\text{net}} = -D_{2,r} \left( \frac{\partial \phi_{2,r}}{\partial r} \right)_{r,r} = D_{2,r} B \frac{\sinh K_{2,r} a + K_{2,r} r_r \cosh K_{2,r} a}{r_r^2} \quad (\text{B-7})$$

$$-D_{2,r} \frac{\frac{\Sigma_{1,r}}{D_{2,r}}}{K_{1,r}^2 - K_{2,r}^2} C \frac{\sinh K_{1,r} a + K_{1,r} r_r \cosh K_{1,r} a}{r_r^2}$$

Applying Eq. (B-4),

$$\frac{D_{1,r} C}{r_r^2} (\sinh K_{1,r} a + K_{1,r} r_r \cosh K_{1,r} a) = - \frac{\eta D_{2,r} B}{r_r^2} (\sinh K_{2,r} a + K_{2,r} r_r \cosh K_{2,r} a) \quad (\text{B-8})$$

$$+ \eta \frac{\frac{\Sigma_{1,r} C}{K_{1,r}^2 - K_{2,r}^2}}{r_r^2} \frac{\sinh K_{1,r} a + K_{1,r} r_r \cosh K_{1,r} a}{r_r^2}$$

Rearranging and solving for B,

$$B = C \left( \frac{\frac{\Sigma_{1,r}}{D_{2,r}}}{K_{1,r}^2 - K_{2,r}^2} - \frac{D_{1,r}}{\eta D_{2,r}} \right) \frac{\sinh K_{1,r} a + K_{1,r} r_r \cosh K_{1,r} a}{\sinh K_{2,r} a + K_{2,r} r_r \cosh K_{2,r} a} \quad (\text{B-9})$$

The negative thermal-neutron current density is given by

$$(J_2)_{r,r}^- = \left( \frac{\phi_{2,r}}{4} + \frac{D_{2,r}}{2} \frac{\partial \phi_{2,r}}{\partial r} \right)_{r,r} = \frac{1}{4} \left( \frac{B \sinh K_{2,r} a}{r_r} - C \frac{\frac{\Sigma_{1,r}}{D_{2,r}} \sinh K_{1,r} a}{K_{1,r}^2 - K_{2,r}^2} \right) \quad (\text{B-10})$$

$$- \frac{D_{2,r}}{2} B \frac{\sinh K_{2,r} a + K_{2,r} r_r \cosh K_{2,r} a}{r_r^2} + C \frac{D_{2,r}}{2} \left( \frac{\frac{\Sigma_{1,r}}{D_{2,r}}}{K_{1,r}^2 - K_{2,r}^2} \right) \frac{\sinh K_{1,r} a + K_{1,r} r_r \cosh K_{1,r} a}{r_r^2}$$

Substituting for  $B$ ,

$$\begin{aligned}
 (J_2)_{r_r}^- = & \frac{1}{4} \left[ C \left( \frac{\frac{\Sigma_{1,r}}{D_{2,r}} - \frac{D_{1,r}}{\eta D_{2,r}}}{K_{1,r}^2 - K_{2,r}^2} \right) \frac{\sinh K_{1,r} a + K_{1,r} r_r \cosh K_{1,r} a}{r_r (1 + K_{2,r} r_r \coth K_{2,r} a)} - C \frac{\frac{\Sigma_{1,r}}{D_{2,r}}}{K_{1,r}^2 - K_{2,r}^2} \frac{\sinh K_{1,r} a}{r_r} \right] \\
 & - \frac{D_{2,r}}{2} C \left[ \left( \frac{\frac{\Sigma_{1,r}}{D_{2,r}} - \frac{D_{1,r}}{\eta D_{2,r}}}{K_{1,r}^2 - K_{2,r}^2} \right) \frac{\sinh K_{1,r} a + K_{1,r} r_r \cosh K_{1,r} a}{r_r^2} \right. \\
 & \left. - \frac{\frac{\Sigma_{1,r}}{D_{2,r}}}{K_{1,r}^2 - K_{2,r}^2} \frac{\sinh K_{1,r} a + K_{1,r} r_r \cosh K_{1,r} a}{r_r^2} \right] \quad (B-11)
 \end{aligned}$$

Rearranging and canceling like terms,

$$\begin{aligned}
 (J_2)_{r_r}^- = & \frac{C}{1 + K_{2,r} r_r \coth K_{2,r} a} \left\{ \frac{\frac{\Sigma_{1,r}}{D_{2,r}}}{(K_{1,r}^2 - K_{2,r}^2) 4 r_r} (K_{1,r} r_r \cosh K_{1,r} a - K_{2,r} r_r \sinh K_{1,r} a \coth K_{2,r} a) \right. \\
 & \left. - \frac{D_{1,r}}{4 \eta D_{2,r} r_r^2} (\sinh K_{1,r} a - K_{1,r} r_r \cosh K_{1,r} a) [r_r - 2 D_{2,r} (1 + K_{2,r} \coth K_{2,r} a)] \right\} \quad (B-12)
 \end{aligned}$$

Substituting for  $B$  in Eq. (B-7),

$$\begin{aligned}
 (J_2)_{r_r}^{\text{net}} = & \frac{D_{2,r}}{r_r} \left[ C \left( \frac{\frac{\Sigma_{1,r}}{D_{2,r}} - \frac{D_{1,r}}{\eta D_{2,r}}}{K_{1,r}^2 - K_{2,r}^2} \right) (\sinh K_{1,r} a + K_{1,r} r_r \cosh K_{1,r} a) \right. \\
 & \left. - C \frac{\frac{\Sigma_{1,r}}{D_{2,r}}}{K_{1,r}^2 - K_{2,r}^2} (\sinh K_{1,r} a + K_{1,r} r_r \cosh K_{1,r} a) \right] \quad (B-13)
 \end{aligned}$$

Simplifying,

$$(J_2)_{r_r}^{\text{net}} = \frac{-D_{1,r} C}{\eta r_r^2} (\sinh K_{1,r} a + K_{1,r} r_r \cosh K_{1,r} a) \quad (\text{B-14})$$

Applying Eq. (B-1) and solving for  $P$ ,

$$P = \frac{1 + K_{2,r} r_r \coth K_{2,r} a}{\frac{K_{1,r}^2}{K_{1,r}^2 - K_{2,r}^2} \frac{\eta r_r}{4D_{2,r}} \frac{K_{1,r} r_r \cosh K_{1,r} a - K_{2,r} r_r \sinh K_{1,r} a \coth K_{2,r} a}{\sinh K_{1,r} a + K_{1,r} r_r \cosh K_{1,r} a} - \frac{r_r - 2D_{2,r} (1 + K_{2,r} r_r \coth K_{2,r} a)}{4D_{2,r}}}$$

(B-15)

## APPENDIX C

### Evaluation of Integral Form for $P_m$

The determination of  $P_m$  involves the evaluation of the integral in Eq. (54):

$$P_m = 2 \int_0^{\theta_{\max}} \cos \theta \sin \theta (1 + e^{-\sum_{a,c} l_c(\theta)}) d\theta \quad (\text{C-1})$$

$$l_c(\theta) = -2r_c \cos \alpha \quad (90^\circ \leq \alpha \leq 180^\circ) \quad (\text{C-2})$$

$$\sin \alpha = \frac{r_r}{r_c} \sin \theta \quad (\text{C-3})$$

Now,

$$\sin \theta_{\max} = \frac{r_c}{r_r} \quad (\text{C-4})$$

$$\cos \alpha = -\sqrt{1 - \sin^2 \alpha} = -\sqrt{1 - \left(\frac{r_r}{r_c}\right)^2 \sin^2 \theta} \quad (\text{C-5})$$

and

$$l_c(\theta) = 2r_c \left[ 1 - \left(\frac{r_r}{r_c}\right)^2 \sin^2 \theta \right]^{\frac{1}{2}}$$

Let

$$x = \sin \theta \quad dx = \cos \theta d\theta$$

Then, Eq. (C-1) becomes

$$P_m = 2 \int_0^{\sin \theta_{\max}} x \left( 1 - e^{-2\Sigma_{a,c} r_c \sqrt{1 - (r_r/r_c)^2 x^2}} \right) dx \quad (C-6)$$

Now, let

$$\xi^2 = 1 - \left( \frac{r_r}{r_c} \right)^2 x^2$$

$$2\xi d\xi = -2 \left( \frac{r_r}{r_c} \right)^2 x dx$$

and Eq. (C-6), upon substitution and interchange of limits, is

$$P_m = 2 \left( \frac{r_c}{r_r} \right)^2 \int_0^1 \xi (1 - e^{-2\Sigma_{a,c} r_c \xi}) d\xi \quad (C-7)$$

Now, (C-6) may be broken into two standard integrals. Integration yields

$$P_m = 2 \left( \frac{r_c}{r_r} \right)^2 \left[ \frac{1}{2} - e^{-2\Sigma_{a,c} r_c} \left( -\frac{1}{2\Sigma_{a,c} r_c} - \frac{1}{(2\Sigma_{a,c} r_c)^2} \right) - \frac{1}{2\Sigma_{a,c} r_c} \right] \quad (C-8)$$

Finally,

$$P_m = \sin^2 \theta_{\max} \left\{ 1 + \frac{2}{(2\Sigma_{a,c} r_c)^2} \left[ e^{-2\Sigma_{a,c} r_c} (2\Sigma_{a,c} r_c + 1) - 1 \right] \right\} \quad (C-9)$$



## APPENDIX D

### Determination of the Final Equations for Fast and Thermal Fluxes in the Reflector

The fast- and thermal-flux distribution can be obtained as functions of the average thermal flux in the core. The only remaining constant to be determined in the flux equations is  $C$ . Solving for  $C$  from Eq. (B-14),

$$C = - \frac{\eta r_r^2}{D_{1,r}} (J_2)_{r_r}^{\text{net}} \frac{1}{\sinh K_{1,r} a + K_{1,r} r_r \cosh K_{1,r} a} \quad (\text{D-1})$$

but  $(J_2)_{r_r}^{\text{net}}$  is given in Eq. (33) as

$$(J_2)_{r_r}^{\text{net}} = \frac{-\Sigma_{a,c} \bar{\phi}_{2,c} V_c}{A_{r_r}} \quad (\text{D-2})$$

or

$$(J_2)_{r_r}^{\text{net}} = - \frac{\Sigma_{a,c} \bar{\phi}_{2,c} r_c^3}{3r_r^2} \quad (\text{D-3})$$

Then,

$$C = \frac{\eta}{D_{1,r}} \frac{\Sigma_{a,c} \bar{\phi}_{2,c} r_c^3}{3} \frac{1}{\sinh K_{1,r} a + K_{1,r} r_r \cosh K_{1,r} a} \quad (\text{D-4})$$

Noting that

$$\eta = \nu \frac{\Sigma_{f,c}}{\Sigma_{a,c}} \quad (\text{D-5})$$

$$C = \frac{\nu \Sigma_{f,c} \bar{\phi}_{2,c}}{3D_{1,r}} r_c^3 \frac{1}{\sinh K_{1,r} a + K_{1,r} r_r \cosh K_{1,r} a} \quad (D-6)$$

Thus, knowledge of the critical concentration to evaluate  $\Sigma_{f,c}$  yields  $C$  as a function of the average thermal-neutron flux in the core.

Substitution of Eq. (D-6) into Eq. (26) gives the fast-neutron-flux distribution in the reflector as a function of average thermal-neutron flux in the core.

$$\frac{\phi_{1,r}}{\bar{\phi}_{2,c}} = \frac{\nu \Sigma_{f,c} r_c^3}{3D_{1,r}} \frac{1}{\sinh K_{1,r} a + K_{1,r} r_r \cosh K_{1,r} a} \frac{\sinh K_{1,r} (r_r + a - r)}{r} \quad (D-7)$$

The thermal-flux distribution in the reflectors is obtained by successive substitution of Eq. (B-9) for  $B$  and Eq. (D-6) for  $C$  into Eq. (39).

$$\frac{\phi_{2,r}}{\bar{\phi}_{2,c}} = \frac{\nu \Sigma_{f,c} r_c^3}{3D_{1,r}} \left[ \left( \frac{\Sigma_{1,r}}{D_{2,r}} - \frac{D_{1,r}}{\eta D_{2,r}} \right) \frac{1}{r} \frac{\sinh K_{2,r} (r_r + a - r)}{\sinh K_{2,r} a + K_{2,r} r_r \cosh K_{2,r} a} - \frac{\Sigma_{1,r}}{K_{1,r}^2 - K_{2,r}^2} \frac{1}{r} \frac{\sinh K_{1,r} (r_r + a - r)}{\sinh K_{1,r} a + K_{1,r} r_r \cosh K_{1,r} a} \right] \quad (D-8)$$

## APPENDIX E

## Summary of Nuclear Parameters Used in the Analysis

The cross sections for the core and reflector are taken from Ref. 8. All constants were evaluated for a reflector temperature of 2500°K, except for the absorption cross section of graphite, which is assumed to have its room-temperature value for conservatism.

$$\sigma_a^{29} = 4 \times 10^3 \text{ barns}$$

$$\sigma_f^{29} = 2.5 \times 10^3 \text{ barns}$$

$$\sigma_a^r = 3 \text{ mbarns}$$

$$\sigma_s^r = 4.8 \text{ barns}$$

The pertinent two-group nuclear constants in the reflector are:

$$K_{1,r}^2 = 1/\tau_r = 4.55 \times 10^{-3} \text{ cm}^{-2}$$

$$K_{2,r}^2 = 1/L_{2,r}^2 = 2.79 \times 10^{-4} \text{ cm}^{-2}$$

$$\Sigma_{2,r} = 2.5 \times 10^{-4} \text{ cm}^{-1}$$

$$D_{2,r} = 0.89 \text{ cm}$$

$$D_{1,r} = 1.11 \text{ cm}$$

$$\Sigma_{1,r} = 5.05 \times 10^{-3} \text{ cm}^{-1}$$

$$\lambda_{tr,r} = 2.67 \text{ cm}$$

The nuclear constants in the core are:

$$\nu = 2.88$$

$$\eta = 1.8$$

January 23, 1962

JET PROPULSION LABORATORY California Institute of Technology • 4800 Oak Grove Drive, Pasadena, California

Recipients of JPL Technical Report  
No. 32-189

SUBJECT: Errata for TR 32-189

Gentlemen:

It is requested that the following changes be made in your copy of Technical Report No. 32-189, entitled "Thermal and Criticality Analysis of the Plasma Core Reactor," by D. F. Spencer, dated January 1, 1962:

1. On page 3 (last line), change  $R_r - R_c$  to  $r_r - r_c$ .
2. On page 6 (Eq. 7, second term on the right), change  $A_m$  to  $A_n$ .
3. On page 10 (2nd paragraph), change 3000 lb/sec to  $1.36 \times 10^6$  g/sec (3000 lb/sec).
4. On page 11, change  $L$  - diffusion length, cm, to  $L$  - length, cm.
5. On page 13 (2nd paragraph), change  $2000^\circ\text{K}$  to  $2500^\circ\text{K}$ .
6. On page 15 (Eq. 24), change  $a$  to  $\alpha$ .
7. On page 17 (Eq. 36, second term on the left), change  $\phi_{1,r}$  to  $\phi_{2,r}$ .
8. On page 18 (Eq. 43, final term), close parenthesis.
9. On page 21 (Eq. 58, first term on the left in numerator), change  $\sinh K_{2,r} (r_r + a + r)$  to  $\sinh K_{2,r} (r_r + a - r)$ .
10. On page 26, add  $L$  - diffusion length, cm.
11. On page 29, substitute attached Fig. 16.
12. On page 40 (Eq. B-12, last term on the right), change  $\sinh K_{1,r} a - K_{1,r} r_r \cosh K_{1,r} a$  to  $\sinh K_{1,r} a + K_{1,r} r_r \cosh K_{1,r} a$ .
13. On page 40 (Eq. B-13, first term on the right), change  $\frac{D_{2,r}}{r_r}$  to  $\frac{D_{2,r}}{r_r^2}$ .

Very truly yours,



N. F. White, Assistant Manager  
Reports Section

IEN/DW:bh

Technical Report No. 32-189, Revised Figure 16.

Achievable engine thrust based on thermal and criticality constraints ( $T_c \geq 20,000^\circ\text{K}$ )

